IEEE Access
Multidisciplinary | Rapid Review | Open Access Journal

Received 15 October 2023, accepted 8 November 2023, date of publication 16 November 2023,
date of current version 28 November 2023.

*Digital Object Identifier 10.1109/ACCESS.2023.3334146*

RESEARCH ARTICLE

# A Case Study on Structural Optimization Design of Shock Absorber Brackets in Automobile Suspension

**YAN LIU[1], LU PAN[1,2], QIANG CUI[1], AND DONGBO MENG[3]**
[1]Anhui Technical College of Mechanical and Electrical Engineering, Wuhu, Anhui 241000, China
[2]Wuhu Metal Matrix Composite Material Laser Additive Manufacturing Engineering Technology Research Cente, Wuhu, Anhui 241000, China
[3]Ideal Automobile Shanghai Technology Company Ltd., Shanghai 201805, China

Corresponding author: Yan Liu (liuyan19851010@163.com)

This work was supported in part by the Key Natural Science Research Projects in Anhui Universities under Grant 2022AH052351 and Grant 2022AH052369, and in part by the Wuhu Science and Technology Bureau Project under Grant KJCXPT202203.

**ABSTRACT** For connecting plate of shock absorber bracket in automobile suspension, lightweight requirement is a mainstream design tendency. Based on the principle of maximum stiffness, this work conducts a case study on structural optimization design of shock absorber brackets in automobile suspension. Firstly, both TI-6AL-4V alloy material and the motion simulation function of Inspire software are employed for use in the investigation. It is expected to simulate the motion state of automobile shock absorber extract the load effectively. Hence, the load is applied to the finite element model of the shock absorber connecting plate as the boundary condition. Then, the software is used to explore the shape control method for the connecting plate under different optimization objectives. Also, the topology optimization is carried out on the premise of 2-factor 4-level orthogonal test, and the extrusion is used as the shape control method. Finally, using 8 mm thickness as constraint condition, the optimized structure with safety factor of 2.3 and weight loss rate of 72.6% can be obtained.

**INDEX TERMS** Structural optimization design, automobile suspension, simulation modeling, manufacturing optimization.

## I. INTRODUCTION

China has set 2030 as the year for carbon peak and 2060 as the year for carbon neutrality [16]. To this end, huge reforms have been made in various industries [17]. Lightweight, as an important measure to save energy and reduce carbon in automobiles, has been included in one of the nine technological development directions of the ''Energy Saving and New energy Vehicle Technology Roadmap 2.0'' [18]. At present, the lightweight design of automobiles mainly starts from the three aspects of material lightweight, structure optimization and changing process [19]. Most of the research focuses on the lightweight design of large structures such as automobile suspension, frame, seat skeleton, etc [20].

Xianchang et al. [1] established a finite element model for the automotive gearbox shell and, through multi-objective topology optimization analysis, strengthened the high-density region and reduced the low-density region, reducing the mass by 7.5% and improving the natural frequency to reduce the resonance risk. Fang et al. [2] based on the beam unit, designed the frame of electric vehicles through 176 iterations of topology optimization, and obtained the final layout of the frame, which reduced the final mass by 10.5% and improved the performance by more than 9.3%. Zhang et al. [3] studied the control arm of automobile suspension by using morphology optimization and topology optimization, and its mass was reduced by 9.3%. Ge et al. [4] realized the mass reduction of the car seat greatly by changing the material and optimizing the topology structure. However, there are few researches on the parts with low mass and more concentrated force in the automobile [21].

The associate editor coordinating the review of this manuscript and approving it for publication was Jingang Jiang.

Since the shock absorber is the main shock absorption part, its force will change with the different pavement environment, which makes it difficult to set the load condition and boundary constraint conditions when using finite element analysis [22]. Altair's Inspire software imparts [5], [6] simulation power to the digital model of the shock absorber so that the shock absorber can be simulated [23]. In addition, the load loading model can be extracted during the motion process, and then the solver [7] of OptiStruct topology optimization module can be directly invoked during the optimization process [24]. After the topology optimization, the optimal force path and material distribution structure can be obtained in the design space [25].

## II. INITIAL ANALYSIS OF THE CONNECTING PLATE

### A. TOPOLOGY OPTIMIZATION THEORY

Continuum topology optimization is a method for optimizing the distribution of materials in a given region under a given load, constraints, and objective function. It helps to improve the strength of the design while reducing the amount of material. Topology optimization methods mainly include variable density method, homogenization method, phase field method and level set method [8]. Because variable density method is easy to realize, convergent and stable, the most mature topology optimization method is variable density method at present, and its mathematical model of topology optimization problem can be expressed as [9] and [10]:

$$\begin{aligned} X &= (\mathrm{x}_1, \ldots\ldots, \mathrm{x}_\mathrm{n})^T \in R \\ C(X) &= U^T KU = \sum\nolimits_{\mathrm{n}=1}^{\mathrm{N}} (\mathrm{x}_\mathrm{n})^{\mathrm{p}} \mathrm{u}_\mathrm{n}^T \mathrm{k}_0 \mathrm{u}_\mathrm{n}, \\ \mathrm{p} &> 1 \\ V &= \sum\nolimits_{\mathrm{n}=1}^{N} \mathrm{x}_\mathrm{n} V_\mathrm{n}, 0 \le \mathrm{x}_\mathrm{n} \le 1 \end{aligned} \tag{1}$$

In the formula: Variable $X$ is the relative density matrix of each element in the working domain, R is the range of the density filter in the mathematical model, the objective function $C(X)$ is the structural flexibility, $U$ is the displacement matrix under constraints in the working domain, $K$ represents the total stiffness matrix of the design model in the working domain, $Un$ is the displacement of the nth element, $Xn$ is the relative density of the nth element, Kn is the optimized stiffness of the nth element, $X_0$ is the initial element density, $p$ is the penalty factor, and $V$ is the optimized volume. Local approximation is used to solve the optimization, and the criteria of regular convergence and soft convergence are followed in the solution process.

### B. MATERIAL INTERPOLATION MODEL

The SIMP material interpolation model can be expressed as.

$$E_\mathrm{i} = P(\eta_\mathrm{i}) E_{\mathrm{i}0} = \eta_\mathrm{i}^{\mathrm{p}} \mathrm{E}_{\mathrm{i}0} \tag{2}$$

where $E_{i0}$ is the elastic modulus of the unit i in the complete entity state ($\eta_i$=1);$P(\eta_i)$ is the interpolation function; p is the penalty coefficient. In the case of inertia load being overload load, the classical SIMP model will cause distortion of the low-density element due to the mismatch between the material mass and the stiffness model. Through the polynomial interpolation model, the following formula can be deduced:

$$E_\mathrm{i} = [(1-\omega)\eta_i^p + \omega\eta_i] E_{i0} \tag{3}$$

where: $\omega$ is the weight coefficient of the linear term. Thus, the ratio of the element mass to the stiffness penalty coefficient is defined as:

$$\mathrm{r}_{\mathrm{mk}} = \frac{1}{(1-\omega)\eta_\mathrm{i}^{\mathrm{p}-1} + \omega} \tag{4}$$

Through the fact that $\omega$ in the denominator, no matter what value $\eta_i$ takes in [0, 1], $r_{mk}$ is of finite size, the problem of unit distortion in the SIMP model is solved [11].

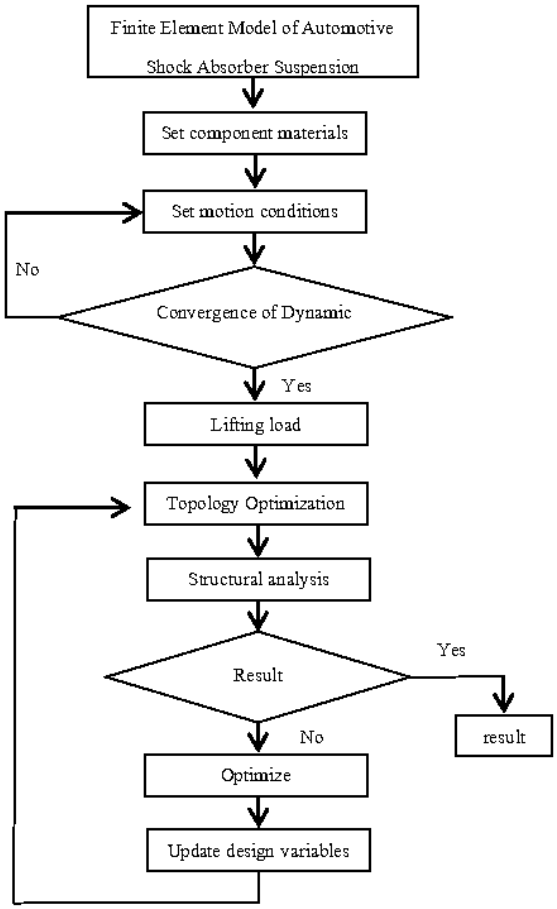


**FIGURE 1.** Structure optimization flowchart.

### C. TOPOLOGY OPTIMIZATION PROCESS

Based on the above optimization theory, Inspire software is used to solve the topology optimization of the shock absorber connecting plate through continuous iteration. Finite element analysis, motion simulation, sensitivity calculation and updating design variables are the iterative calculation processes [12]. After convergence, the optimal structure is obtained. The flowchart of lightweight design of automotive suspension shock absorber connection plate is shown in Figure 1.

**TABLE 1.** Material properties of Ti-6Al-4V alloy.

| YOUNG'S MODULUS E/MPa | POISSON'S RATIO Nu | DENSITY Kg/mm | YIELD STRESS MPa | COEFFICIENT OF THERMAL EXPANSION $\alpha$ /K |
|---|---|---|---|---|
| 116522 | 0.31 | 4.429 ×10 | 827 | 8.82 ×10 |

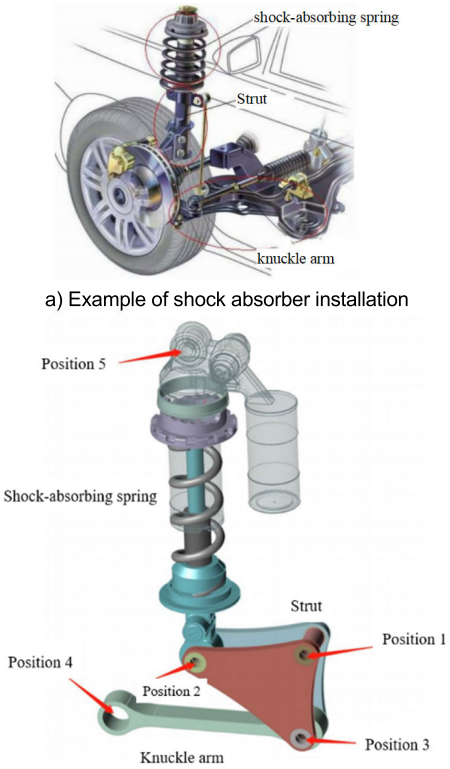


**FIGURE 2.** Digital model of shock absorber.

## III. DIGITAL MODEL ANALYSIS OF SHOCK ABSORBER CONNECTION PLATE

### A. MOTION ANALYSIS AND BOUNDARY CONDITION SETTING

The shock absorber is installed on the chassis suspension, and it is installed in parallel with the elastic element. The digital model is shown in Figure 2 (a).Its main function is to accelerate the attenuation of frame and body vibration, in order to improve the ride comfort of the car. The load state of the shock absorber in the driving state, the position 4 is connected with the wheel, the position 5 is connected with the chassis in a relatively fixed state, so it is set to ground articulated, and the position 1,2,3 is activated articulated. In addition, a translational motor is set to simulate the force on the chassis suspension in the process of car driving. The operational point of the translational motor is the center of the cylinder of the cushion ring, acting on the YZ plane, and the Angle of the -Z axis is 60° (direction vector x= 0; y=0.866025; z=−0.5), the drive type is displacement, and the design requires a safety factor of not less than 1.4.

**TABLE 2.** Initial strength analysis results.

| MINMUNM SAFETY FACTOR | MAXIMUM DISPLACEMENT/mm | MAXIMUM RICE SETH STRESS /MPa |
|---|---|---|
| 9.2 | 0.06394 | 90.34 |

### B. MATERIAL ANALYSIS

The purpose of lightweight design is to make the shock absorber maintain good working performance on the basis of reducing the mass, the choice of materials is particularly important, for which Ti-6Al-4V alloy is used, which is $\alpha + \beta$ titanium alloy with excellent heat resistance, corrosion resistance, specific strength and good biocompatibility. The properties of alloy material Ti-6Al-4V are shown in Table 1.

- At present, there have been more application research in the field of aviation and medicine. The Ti-6Al-4V alloy developed by Pan et al. [13] et al. by laser melting deposition technology has a tensile strength of 1191MPa, a yield strength of 1129MPa and a elongation of 8.3%. It provides a reliable basis for printing optimized shock absorber parts by laser powder bed melting process. The initial structural mass of the shock absorber connecting plate is 220g before it is lightened.

### C. ANALYSIS OF INITIAL LOAD

After motion simulation, the transient force and load at any position on the shock absorber component can be obtained within 2 seconds. Figure 2 (b) specific analysis of the force load at position 1, position 2 and position 3, the transient resultant force at the three positions is shown in Figure 3. Hinged 16, 17, 18 corresponding to positions 1,2,3. Through the comparison between the transient force diagram and the motion state, it is concluded that the three hinged joints are subject to the maximum resultant force and torque when the motor displacement is the smallest.

### D. STRENGTH ANALYSIS

After the motion simulation, the motion load is obtained, and the initial strength analysis of the shock absorber components is carried out. The size of the analysis unit was set to 2mm, the motion time was set to 2 seconds during the motion analysis, and the output power was 30Hz. The load on the shock absorber components on 60 time samples was obtained as the analysis condition. The initial structural strength analysis was carried out by Inspire software, and the minimum safety factor, maximum displacement and maximum Rice equivalent stress were obtained, as shown in Table 2.

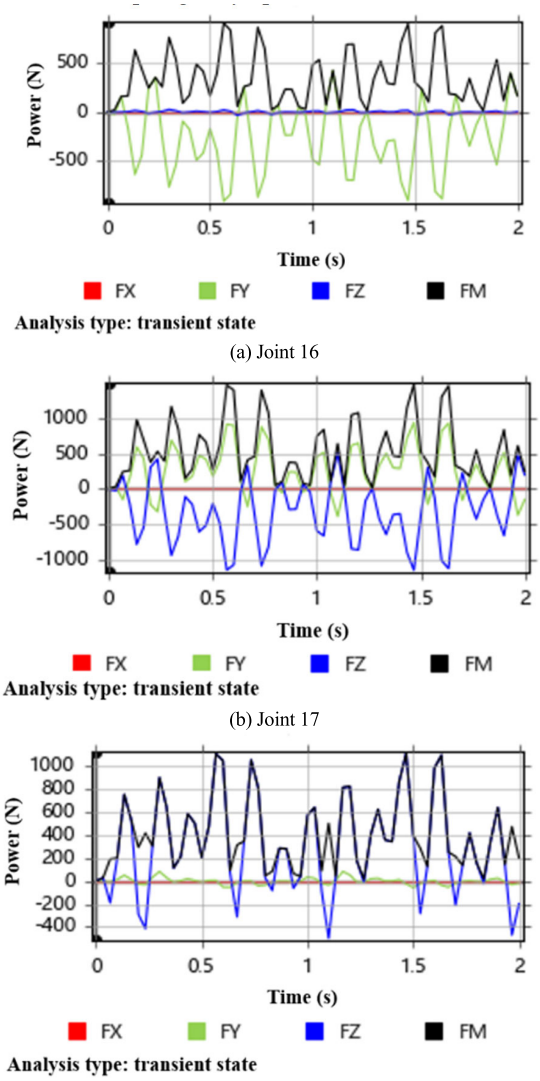


**FIGURE 3.** Transient stress diagram at hinge joint.

## IV. SHAPE CONTROL SCHEME SELECTION

After topological optimization of the two side connecting plates, Inspire will find the best material distribution results on the two side connecting plates according to constraints to achieve structural optimization. However, considering the overall assembly requirements of the shock absorber, positions 1, 2 and 3 of the shock absorber need to be hinged with other parts, and the internal holes at these three positions must ensure the integrity of the structure. At this time, the hinged hole structure needs to be properly extended, separated and other operations to make the installation hole structure independent as a non-design space, while the rest are design Spaces can be topologically optimized.

As shown in Figure 4 (a), uneven material distribution will occur after multiple iterations of the conceptual model, resulting in material missing in many parts of the generated conceptual model, and even material protruding that cannot connect and support. At this time, further topology optimization is needed, and the method of adjusting the topology

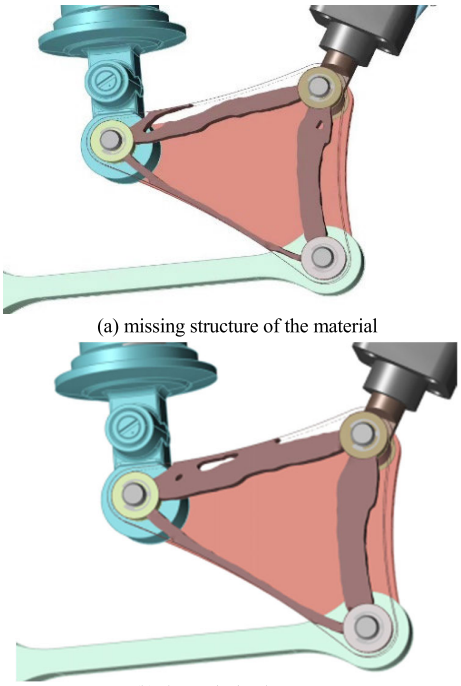

(a) missing structure of the material

(b) the optimized structure

**FIGURE 4.** Change graph of topology optimization structure.

slider is used for iterative optimization again, and the overall material will be optimized with the optimization. Adjusting the topological slider on the premise of uniform material distribution and reasonable structure will lead to a certain difference between the quality of the final conceptual model and the initial quality target. FIG. 4 (a) is an unadjusted conceptual model after optimization. Due to its unreasonable structure, the topological slider needs to be adjusted again, and the conceptual model as shown in FIG. 4 (b) is finally obtained. The irrational structure is improved, but its quality is increased by 2%.

As the main part of automobile vibration reduction, its maximum stiffness is taken as the constraint condition of optimization, and its mass percentage, optimized thickness constraint value and shape control scheme are all important factors affecting the optimization results. The optimal thickness is set as 8mm in the first test, and 6 groups of tests are set with various shape control methods as variables. The best shape control method was obtained through the first test. The test results are shown in Table 3. Through the test, it is found that the safety factor of scheme 3 is 2.8 after optimization, while scheme 6 has the minimum displacement after optimization, and the displacement is 0.004858mm. Both of these schemes can reach the design goal with a safety factor greater than 1.4. From this, it can be analyzed that the methods of extrusion in scheme 3 and symmetric stamping in scheme 6 can obtain better optimization results, but their thickness is also one of the important factors affecting the optimization results.

Therefore, on the basis of scheme 3 and scheme 6, orthogonal tests [14] of 2 factors and 4 levels are carried out. The

**TABLE 3.** First test.

| SERIAL NUMBER | SHAPE CONTROL | SAFETY FACTOR | MISES EQUIVALENT STRESS /MPa | | DISPLACEMENT /mm | |
|---|---|---|---|---|---|---|
| | | MIN | MAX | MIN | MIN | MAX |
| 1 | SYMMETRICAL+TWO-WAY DRAWING | 2.5 | 332.7 | 2.613 | 0.02347 | 0.5517 |
| 2 | ONE WAY DRAWING DIE | 2.6 | 324 | 2.489 | 0.01929 | 0.4352 |
| 3 | SQUEEZE | 2.8 | 299.4 | 3.431 | 0.02012 | 0.4331 |
| 4 | SYMMETRY+RADIATION | 1.8 | 453.6 | 0.2544 | 0.01445 | 0.2152 |
| 5 | HANGING IN THE AIRr | 1.3 | 617.7 | 5.85 | 0.009184 | 0.6143 |
| 6 | SYMMETRY+STAMPING | 2.4 | 349.2 | 3.399 | 0.004858 | 0.2765 |

**TABLE 4.** Orthogonal test.

| SERIAL NUMBER | SHAPE CONTROL | MINIMUM THICKNESS /mm | QUALITY OBJECTIVES | SAFETY FACTOR | MISES EQUIVALENT STRESS /MPa | | DISPLACEMENT /mm | PART MASS /g |
|---|---|---|---|---|---|---|---|---|
| | | | | Min. | Max | Min | Max | |
| 1 | EXTRUSION | 5 | 20% | 1.5 | 556.4 | 0.0002801 | 0.5879 | 72.635 |
| 2 | | | 25% | 2.2 | 368.7 | 4.439 | 0.4473 | 71.11 |
| 3 | | | 30% | 2 | 404.5 | 4.175 | 0.521 | 65.173 |
| 4 | | | 35% | 1.4 | 605.8 | 0.0002023 | 0.7907 | 54.257 |
| 5 | | 6 | 20% | 2 | 411.2 | 0.008562 | 0.5027 | 67.553 |
| 6 | | | 25% | 1.5 | 553.3 | 0.0007552 | 0.7693 | 52.946 |
| 7 | | | 30% | 2.7 | 312 | 3.714 | 0.3195 | 82.966 |
| 8 | | | 35% | 3.8 | 219.9 | 2.671 | 0.2654 | 101.26 |
| 9 | | 7 | 20% | 2.6 | 321 | 3.717 | 0.4504 | 66.788 |
| 10 | | | 25% | 2.6 | 317.5 | 1.993 | 0.4146 | 72.577 |
| 11 | | | 30% | 1.7 | 497.2 | 1.897 | 0.4846 | 64.682 |
| 12 | | | 35% | 2.8 | 291.9 | 5.578 | 0.3558 | 75.113 |
| 13 | | 8 | 20% | 2.3 | 358.3 | 8.316 | 0.5948 | 51.929 |
| 14 | | | 25% | 3 | 271.5 | 6.103 | 0.3901 | 68.194 |
| 15 | | | 30% | 2.5 | 325.1 | 0.00004628 | 1553000 | 65.543 |
| 16 | | | 35% | 2.8 | 298.4 | 3.506 | 0.2731 | 91.303 |
| 17 | SYMMETRY +STAMPING | 5 | 20% | UNABLE TO RECONSTRUCT | | | | |
| 18 | | | 25% | 0.6 | 1361 | 6.594 | 0.7566 | 51.484 |
| 19 | | | 30% | 0.9 | 943.7 | 6.21 | 0.4251 | 63.835 |
| 20 | | | 35% | 1 | 870.7 | 5.128 | 0.4275 | 63.833 |
| 21 | | 6 | 20% | 0.8 | 1024 | 0.01786 | 0.9968 | 43.393 |
| 22 | | | 25% | 1.1 | 776.1 | 5.166 | 0.8064 | 58.666 |
| 23 | | | 30% | 1.7 | 478.7 | 4.391 | 0.2877 | 78.043 |
| 24 | | | 35% | 2.3 | 364.7 | 2.87 | 0.2196 | 92.056 |
| 25 | | 7 | 20% | 0.7 | 1226 | 0.0003731 | 5830000 | 42.703 |
| 26 | | | 25% | 1.7 | 476.8 | 4.14 | 0.5328 | 56.931 |
| 27 | | | 30% | 1.7 | 474.7 | 3.333 | 0.3034 | 76.722 |
| 28 | | | 35% | 3.3 | 253.8 | 5.979 | 0.2252 | 90.69 |
| 29 | | 8 | 20% | 0.4 | 1925 | 7.897 | 1.184 | 40.182 |
| 30 | | | 25% | 0.8 | 998.6 | 7.656 | 0.5606 | 54.689 |
| 31 | | | 30% | 2.7 | 302.4 | 4.787 | 0.3559 | 67.809 |
| 32 | | | 35% | 2.9 | 285.6 | 4.705 | 0.2535 | 80.808 |

2 factors are respectively the percentage of optimized mass and the optimized thickness constraint value, and 4 levels are selected for each factor. The mass percentage is 20%, 25%, 30% and 35% respectively, and the optimized thickness

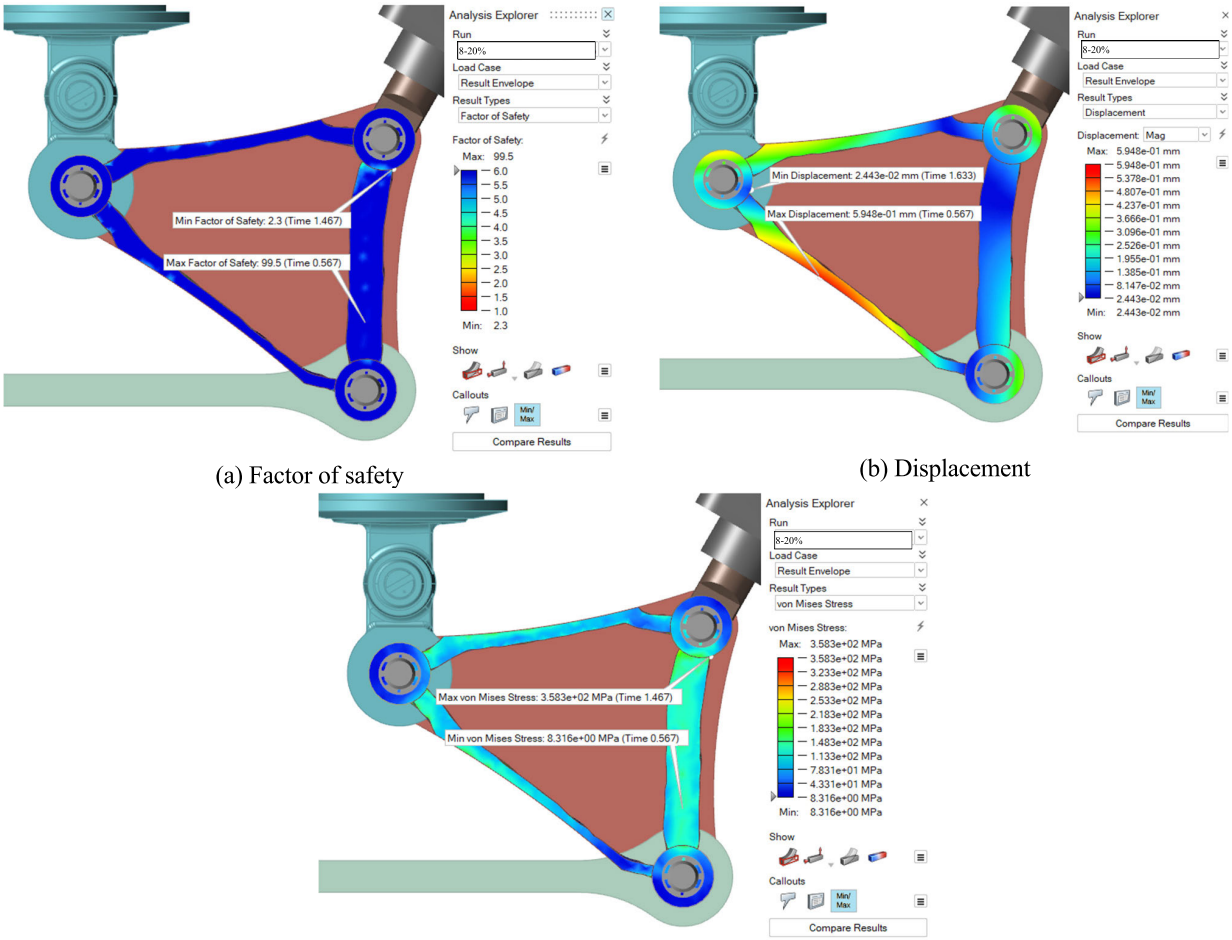


**FIGURE 5.** **Optimized performance analysis cloud.**

is 5, 6, 7 and 8mm respectively. It can be seen from Table 4 that after the final optimization with extrusion as shape control and symmetrical stamping as shape control, the structural safety factor has met the initial optimization design requirements to reach more than 1.4, but the mechanical properties of the extruded structure are obviously better. From the analysis results in Table 4, it can be seen that the optimized weight of plan 6 and Plan 13 is 52.946g and 51.929g respectively, and the weight reduction is as high as 76% and 84%.

Moreover, the maximum displacement and minimum safety factor both meet the design requirements. Among them, scheme 13 has a higher safety factor and a smaller maximum displacement. The key performance of scheme 13 after optimization is shown in the following figure. It can be seen from Figure 5 that at this time, when the connecting plate of the automobile vibration damping is 0.567s in the 2s cycle of simulation operation, the maximum displacement of 0.5948mm will occur in the smaller part of the lower bracket, and the maximum safety factor of 99.5 and the minimum Mises equivalent stress of 8.316Mpa will occur on the right bracket. At 1.467s, the maximum Mises equivalent stress is 358.3Mpa at the junction of the engine and components, resulting in the minimum safety factor of 2.3 here.

Based on the above analysis, it can be seen that the topology optimization effect of scheme 13 is better, but the maximum displacement of scheme 13 is increased by 365% and the minimum safety factor is reduced by 50%, indicating that although the mass of shock absorber components is significantly reduced after optimization, its mechanical properties become worse.

## V. VERIFICATION OF MOTION AND GEOMETRIC RECONSTRUCTION

Based on the optimization results of scheme 13, the motion simulation of the shock absorber is carried out again. In Figure 6, the red lines are the motion tracks of the three hinged positions of the shock absorber components. Comprehensive analysis shows that the hinged 16 moves to 0.567s. At the maximum displacement in the Z direction, the maximum resultant force is 909.77N, and the maximum safety factor appears at the right support of the shock absorber, while hinged 17 receives the maximum resultant force of 1466.7N at 1.467s, while hinged 18 receives the maximum resultant force of 1117N. At this time, the right bracket near the mounting hole of hinged 17 will produce the maximum rice stress, resulting in the minimum safety factor.

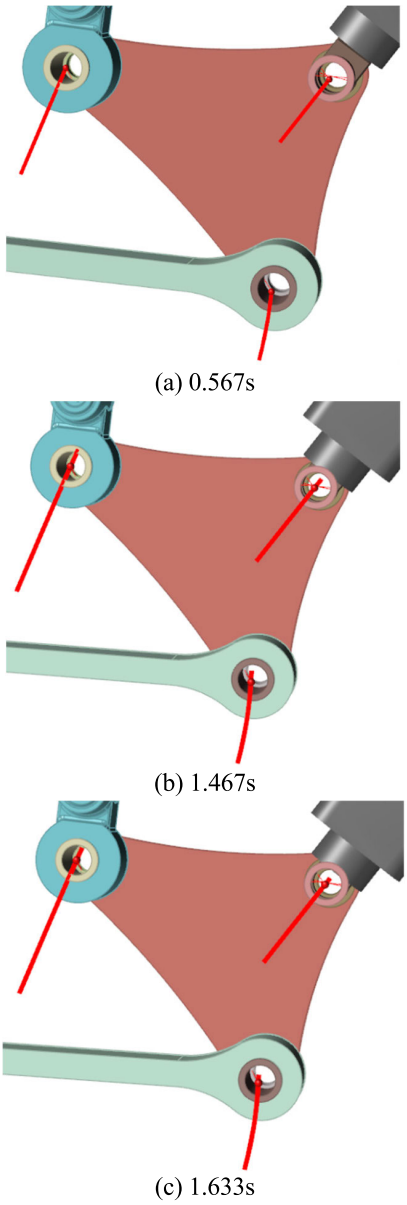


**FIGURE 6.** Scheme 13 is the transient stress diagram of the hinge joint.

The conceptual model based on optimal scheme 13 was directly reconstructed [15], [16] using the PolyNURBS tool in Inspire software. The resulting geometric model not only met the design requirements but also met the aesthetic requirements, so the model needed to be smootened. The number of iterations was changed to 40, the number of PolyNURBS surfaces was changed to 1000, and the ''intersection'' option was selected to realize the fairing of the reconstructed model and the three mounting holes in the non-design space. Through the merging method of Boolean operation, the reconstructed model and the mounting holes can be recombined to obtain the manufacturable geometric model.

After geometric reconstruction, the connecting parts of the shock absorber are checked again to meet the

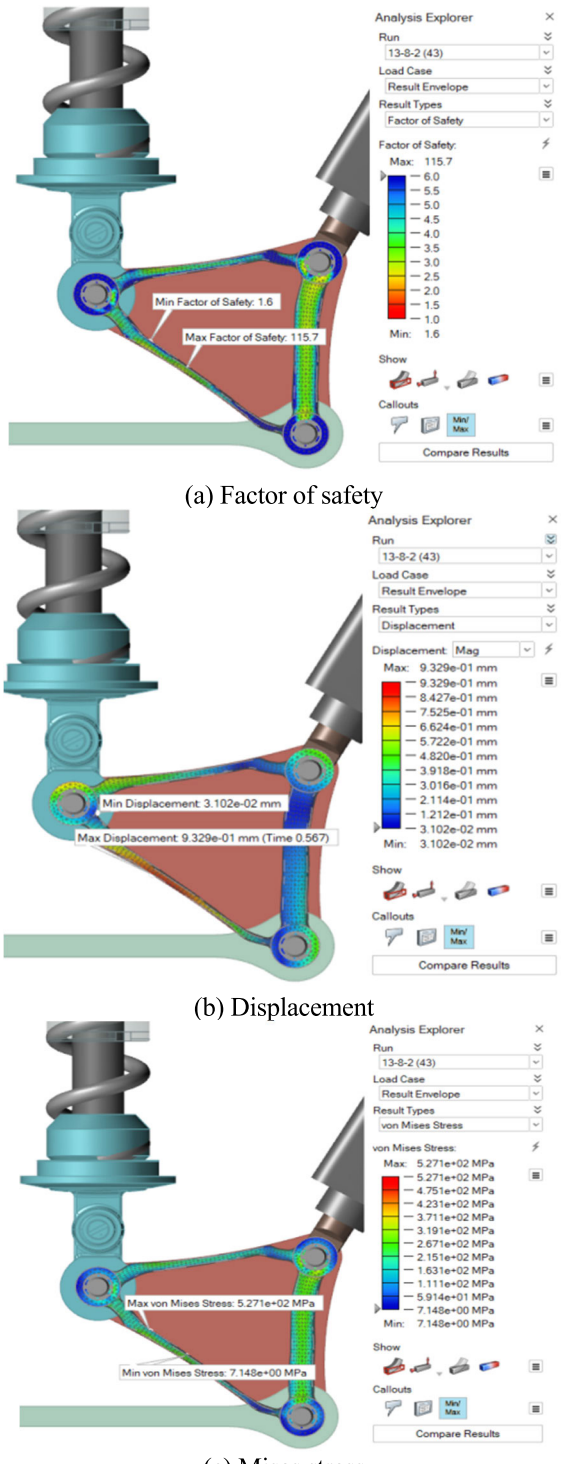


**FIGURE 7.** Post-geometric reconstruction performance analysis nephogram.

motion requirements of the shock absorber, and then the strength is checked again. The size of the analysis unit is 2mm, and each connection adopts 2 loads as the parameter for the final strength check. The strength check analysis results are shown in Figure 7. The lightweight component has been checked three times by the initial


(a) original model quality


(b) optimization of model quality

**FIGURE 8.** Optimizing effect of 3D print quality.

model-conceptual model-reconstructed model. The data are shown in Table 5. Through three times of data analysis and comparison, it is found that the final strength of the optimized component has decreased and the maximum displacement has been achieved.As the quantity increases, the safety factor also decreases, but both meet the design requirements, and the structure is optimized, and the material accumulation is greatly reduced compared with the original part, at this time the mass is 60.3g.

## VI. QUALITY ERROR ANALYSIS OF ADDITIVE MANUFACTURING

Based on the topology optimization model structure above, UPBox + printer was used to print the self-supplied PLA,

**TABLE 5.** Initial model-conceptual model-refactoring model performance comparision table.

| | MINIMUM SAFETY FACTOR | MAXIMUM DISPLACEMENT /mm | MAXIMUM RICE SETH EQUIVALENT STRESS /MPa |
|---|---|---|---|
| INITIAL MODEL | 9.2 | 0.06394 | 90.34 |
| CONCEPTUAL MODEL | 2.3 | 0.5948 | 358.3 |
| REFACTORING MODEL | 1.6 | 0.9329 | 527.1 |

**TABLE 6.** Quality comparision table.

| | OPTIMIZE THE PREQUALITY /g | OPTIMIZE THE POST QUALITY /g | RATE OF CHANGE |
|---|---|---|---|
| THEORETICAL MODEL | 220 | 60.3 | 72.6% |
| 3D MODEL | 63.7 | 16.5 | 74% |
| RELATIVE ERROR | - | - | 1.4% |

and the optimized digital model was imported into the software through STL file for printing. The weight of the two physical models trial-produced by 3D printing was shown in Figure 8. The comparison of the theoretical quality and 3D printing quality of the automotive shock absorber before and after optimization is shown in Table 6. As can be seen from the table,the theoretical quality of the optimized front and rear bracket was reduced by 72.6%, and the quality of the optimized front and rear bracket 3D printing model was reduced by 74%, with a relative error of 1.4%. The results show that the 3D printing processing method has a good ability to control the processing error.

## VII. CONCLUSION

Through the orthogonal test of 2 factors and 4 levels, the optimization model of shock absorber components with good overall performance is analyzed, and the strength check data discrimination after its geometric reconstruction can be obtained:

(1) For the connecting rod of the automobile shock absorber, after extracting the load while simulating the motion and applying it to the boundary of the digital shock absorber model as the constraint condition, it is concluded under the verification of the orthogonal test that the maximum stiffness is the target, the mass constraint is 20%, the minimum thickness is set to 8mm, and the shape control method of extrusion can get a higher weight loss. The optimized structure with relatively good mechanical properties.

(2) After optimization, the overall quality of the automobile shock absorber connection plate is reduced to 60.3g, and the weight loss rate is as high as 72.6%.

(3) After optimization, the mechanical performance of the shock absorber connection plate has decreased, but it still meets the design requirements, and the safety factor is greater than 1.4.

(4) Through the strength analysis, it can be seen that the load of the shock absorber connecting plate is mainly

distributed in the position of the hinged connecting rod at the three places, and the middle of the connecting plate is the material redundancy area.

(5) The maximum displacement can be seen that its structure is relatively weak, and the load near the installation hole position at the hinged 17 is large, resulting in a low safety factor, and the two structures can be re-optimized in the later stage

## REFERENCES

[1] X. Peng, W. Cai, Z. Lin, and B. Gao, "Static and dynamic analysis and topology optimization design of gearbox shell of electric vehicle," *J. Mech. Transmiss.*, vol. 45, no. 7, pp. 74–81, 2021.
[2] C. Fang, S. Zhao, G. Yan, and G. Qin, "Multi-objective topology optimization-size optimization-fine design of electric vehicle frame," *Mach. Des. Manuf.*, no. 8, pp. 16–22, 2023.
[3] Z. Zhang, R. Chen, Z. Xu, Y. He, and W. Li, "Research on topology optimization of multi-objective vehicle suspension control arm," *Chin. J. Mech. Eng.*, vol. 53, no. 4, pp. 114–121, 2017.
[4] H. Ge, G. Li, J. Lou, W. Xiong, and Z. Xiao, "Lightweight design of automotive seat frame based on topology optimization," *J. Ningbo Univ., Sci. Technol. Ed.*, pp. 1–6, 2023.
[5] M. Yang, J. Yu, and Y. Guo, "Research status and development trend of automotive suspension shock absorber," *Eng. Test*, vol. 59, no. 2, pp. 94–100, 2019.
[6] L. Wan, Y. Yu, S. Chen, L. Li, and W. Shangguan, "Optimization method of buffer block structure of automobile suspension shock absorber," *J. Chongqing Univ.*, vol. 42, no. 12, pp. 13–22, 2020.
[7] W. Lu, X. Qin, and Y. Zhang, "Lightweight optimization design of motorcycle shock absorber connectors based on inspire," *J. Henan Inst. Eng.*, vol. 35, no. 1, pp. 37–43, 2023.
[8] S. Yang and B. Wang, "Lightweight structural design optimization method for lightweight mechanical arm," *China Mech. Eng.*, vol. 27, no. 19, pp. 2575–2581, 2016.
[9] G. Zhang, L. Xu, D. Li, and X. Wang, "Research on lightweight design method of 3D printing for robot arm based on variable density method," *Machinery Des. Manuf.*, no. 11, pp. 80–84, 2022.
[10] H. Li, W. Yan, Y. Chen, C. Zhang, and Z. Liao, "Lightweight design of four-rotor UAV fuselage based on topology optimization," *Eng. Plastics Appl.*, vol. 51, no. 2, pp. 60–66, 2023.
[11] R. Wang, Z. Xie, Z. Yang, and W. Yu, "Topology optimization of launch support for tower of weapon station based on variable density method," *J. Mil. Equip. Eng.*, vol. 3, no. 44, pp. 60–67, 2023.
[12] Z. Wang, L. Hui, and C. Jian, "Multi-performance constrained topology optimization design of four-rotor UAV frame structure," *Mach. Des. Res.*, vol. 38, no. 6, pp. 173–176, 2022.
[13] L. Pan, H. Zhang, T. Liu, D. Nie, and X. Sun, "Topology optimization and laser additive manufacturing of humanoid robot leg," *Appl. Laser*, vol. 43, no. 2, pp. 47–55, 2023.
[14] G. Shi, X. Wang, Y. Chen, and Z. Du, "Effect of laser power on microstructure and properties of Ti-6Al-4V-0.25C alloy deposited by laser melting," *Rare Metal Mater. Eng.*, vol. 51, no. 12, pp. 4570–4578, 2022.
[15] C. Chen, H. Chen, S. Wu, and J. Wang, "Structural optimization of industrial robot arm based on orthogonal test," *Mach. Tool Hydraul.*, vol. 49, no. 5, pp. 20–24, 2021.
[16] F. Yang, Y. Fan, and P. Li, "Inspire software based on control support structure optimization design," *J. Xi'an Aeronaut. Univ.*, vol. 37, no. 1, pp. 32–37, 2019.
[17] H. Yang, X. Wen, Y. Yu, G. Shi, Z. Wang, Y. Li, A. Zhang, and C. Guo, "A D-band waveguide diplexer based on copper additive manufacturing," *IEEE Trans. Compon., Packag., Manuf. Technol.*, vol. 13, no. 8, pp. 1271–1277, Aug. 2023, doi: 10.1109/TCPMT.2023.3298966.
[18] H.-C. Tran, Y.-L. Lo, H.-C. Yang, H.-C. Hsiao, F.-T. Cheng, and T.-H. Kuo, "Intelligent additive manufacturing architecture for enhancing uniformity of surface roughness and mechanical properties of laser powder bed fusion components," *IEEE Trans. Automat. Sci. Eng.*, vol. 20, no. 4, pp. 2527–2538, Oct. 2023, doi: 10.1109/TASE.2022.3204847.
[19] M. Norouzi, D. C. Saha, H. Jahed, and N. Masoumi, "A phase variation-based smart structure for crack detection on metals using cold spray additive manufacturing," *IEEE Trans. Instrum. Meas.*, vol. 72, pp. 1–10, 2023, doi: 10.1109/TIM.2021.3132994.
[20] I. Sanz-Pena, H. Jeong, and M. Kim, "Personalized wearable ankle robot using modular additive manufacturing design," *IEEE Robot. Autom. Lett.*, vol. 8, no. 8, pp. 4935–4942, Aug. 2023, doi: 10.1109/LRA.2023.3290529.
[21] S. Singh, T. Payarou, M. Boby, J.-M. Lamarre, F. Bernier, M. Ibrahim, and P. Pillay, "Cold-spray additive manufacturing of a petal-shaped surface permanent magnet traction motor," *IEEE Trans. Transport. Electrific.*, vol. 9, no. 3, pp. 3636–3648, Sep. 2023, doi: 10.1109/TTE.2022.3233779.
[22] X. Zhu, J. Tang, Y. Wu, X. Jiao, R. Nygaard, D. Cercone, and H. Xiao, "Glass additive and subtractive manufacturing of a fiber optic rotary encoder for downhole pressure sensing," *IEEE Sensors J.*, vol. 23, no. 7, pp. 6969–6975, Apr. 2023, doi: 10.1109/JSEN.2023.3244494.
[23] M. Ho, S. P. M. Nagaraja, R. U. Tok, A. Rangchian, P. Kavehpour, Y. E. Wang, and R. Candler, "Additive manufacturing with strontium hexaferrite-photoresist composite," *IEEE Trans. Magn.*, vol. 59, no. 6, pp. 1–7, Jun. 2023, doi: 10.1109/TMAG.2019.2963184.
[24] N. Simpson, G. Yiannakou, H. Felton, J. Robinson, A. Arjunan, and P. H. Mellor, "Direct thermal management of windings enabled by additive manufacturing," *IEEE Trans. Ind. Appl.*, vol. 59, no. 2, pp. 1319–1327, Mar. 2023, doi: 10.1109/TIA.2022.3209171.
[25] E. Ottonello, M. Baggetta, G. Berselli, and A. Parmiggiani, "Design and validation of a push-latch gripper made in additive manufacturing," *IEEE/ASME Trans. Mechatronics*, vol. 28, no. 4, pp. 2083–2091, Aug. 2023, doi: 10.1109/TMECH.2023.3276073.

**YAN LIU** was born in Wuhu, Anhui, China, in 1985. She received the master's degree from the Xi'an University of Technology, China. She is currently with the Anhui Technical College of Mechanical and Electrical Engineering. Her research interests include mechanical manufacturing and welding materials.

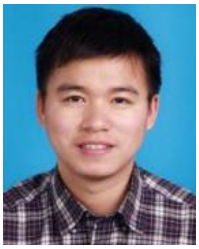

**LU PAN** was born in Taizhou, Jiangsu, China, in 1985. He received the master's degree from the Taiyuan University of Science and Technology, in 2012. He is currently with the Anhui Technical College of Mechanical and Electrical Engineering. His research interest includes metal additive manufacturing.

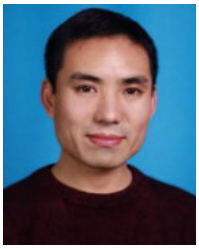

**QIANG CUI** was born in Jiaozhou, Shandong, China, in 1982. He received the bachelor's degree from Shandong University and Law, in 2005. He is currently with the Anhui Technical College of Mechanical and Electrical Engineering. His research interest includes mechanical manufacturing.

**DONGBO MENG** was born in Weinan, Shanxi, China, in 1986. He received the master's degree from the Xi'an University of Technology, China. He is currently with Ideal Automobile Shanghai Technology Company Ltd. His research interests include mechanical manufacturing and automotive safety systems.